



## Research Article

# Surface engineering for enhanced wicking: The role of laser machining and surface roughness

Elham Lori Zoudani, Nam-Trung Nguyen \*\*, Navid Kashaninejad \*

Queensland Micro- and Nanotechnology Centre, Nathan Campus, Griffith University, 170 Kessels Road, Brisbane, QLD, 4111, Australia

## ARTICLE INFO

## Keywords:

Wicking  
Laser machining  
Surface roughness  
Capillary flow  
Wettability  
Microchannels

## ABSTRACT

Wicking is an efficient liquid-handling strategy used in biomedicine, textile engineering, and environmental monitoring. Laser micromachining is a powerful method that induces unidirectional wicking by altering a surface's physical and chemical properties in one step. This research examines how laser machining affects the wicking dynamics of open microchannels. Microchannels were fabricated on a pre-laser-machined hydrophobic square on a silicon substrate, and their wicking performance, i.e., flow rate, water meniscus shape, and durability, was evaluated under various conditions, including different laser parameters, channel orientation, and engraving designs. Depending on its distribution, surface roughness, influenced by laser parameters, is critical in enhancing or hindering wicking. The laser can create two distinct wicking modes on a single platform. Increased roughness slows wicking in horizontally oriented channels, while in vertically oriented channels, it significantly boosts the capillary rate. The durability of wicking also depends on surface roughness properties; microchannels with tightly structured textures maintain durable wicking independent of their capillary flow rate. This study provides insights into how laser machining influences wicking dynamics in microstructures, offering strategies for optimizing microfluidic devices.

## 1. Introduction

Wettability changes can be achieved by modifying either the morphology or chemistry of surface structures [1]. The wetting behavior of a surface is characterized by the contact angle of a water droplet placed on it. According to this definition, a surface is considered superhydrophobic if the measured contact angle exceeds 150°, hydrophobic if the contact angle ranges between 90° and 150°, hydrophilic when it is less than 90°, and superhydrophilic if the contact angle is lower than 10°, indicating a high degree of wickability.

Wicking generally refers to capillary-driven fluid flow resulting from the interplay between adhesive forces at the liquid-solid interface and cohesive forces among fluid molecules [2]. This phenomenon is commonly observed in nature, with a notable example being the absorption of water by plants through their roots in the soil. Wicking enables passive water flow without any external force or power, resulting in a low-cost and simple liquid transport system for a broad range of applications. The wicking behavior of a platform is influenced by factors

such as liquid surface tension and surface properties [3].

Achieving a system with these properties is challenging. Laser machining offers a rapid and efficient method for creating such a platform through single-step processing. This technique allows for the modification of both surface morphology and chemistry [4]. Immediately after laser machining on metals, the resulting structures exhibit superhydrophilic properties with varying degrees of wettability. The heat generated during the laser ablation process induces these changes in wettability [5].

The wicking performance of fluid in a microchannel is generally characterized by the flow rate, the distance travelled by the fluid over time, and the overall flow pattern. Beyond its capability of generating micro- and nano-scale patterns, laser machining has significant potential to induce varied modes of wicking on metallic surfaces. This capability allows for precise control and manipulation of the wicking behavior within microchannels.

With the significant advancement in laser micro/nano manufacturing methods, various studies proposed new ways to enhance

Peer review under responsibility of Vietnam National University, Hanoi.

\* Corresponding author.

\*\* Corresponding author.

E-mail addresses: [nam-trung.nguyen@griffith.edu.au](mailto:nam-trung.nguyen@griffith.edu.au) (N.-T. Nguyen), [n.kashaninejad@griffith.edu.au](mailto:n.kashaninejad@griffith.edu.au) (N. Kashaninejad).

<https://doi.org/10.1016/j.jسامd.2024.100819>

Received 17 September 2024; Received in revised form 13 November 2024; Accepted 17 November 2024

Available online 19 November 2024

2468-2179/© 2024 Vietnam National University, Hanoi. Published by Elsevier B.V. This is an open access article under the CC BY license (<http://creativecommons.org/licenses/by/4.0/>).

laser-induced wicking [6–8]. Fang et al. linked the wicking performance of microgroove structures to temperature, demonstrating the dependency of wicking behavior on temperature [9]. Additionally, some researchers developed bioinspired structures to achieve the desired capillary flow performance through morphological alteration [10,11]. Recently, Huang et al. fabricated gradient-patterned microgrooves to control capillary fluid flow on surfaces [12]. The team demonstrated an enhancement in the capillary rising performance of these step-gradient structures compared to non-gradient ones.

While previous works primarily focused on controlling wicking through factors such as geometries [13,14], surface chemical properties

[4,15,16], or applied heat [17–19], the present study aims to explore a different perspective on the concept of laser-induced wicking by positioning the laser as the sole determinant of wicking dynamics.

This paper addresses the parameters affecting wicking behavior, i.e., flow rate and flow pattern in a microchannel, followed by an examination of wicking durability. A microstructure comprising inlet and outlet circles connected by a microchannel was laser-textured on a pre-machined hydrophobic background to confine water flow within the microchannel. First, the roles of various laser parameters, including laser power, speed, the number of laser passes, and the type of scanning lines (linear, spiral), were investigated for the horizontally oriented

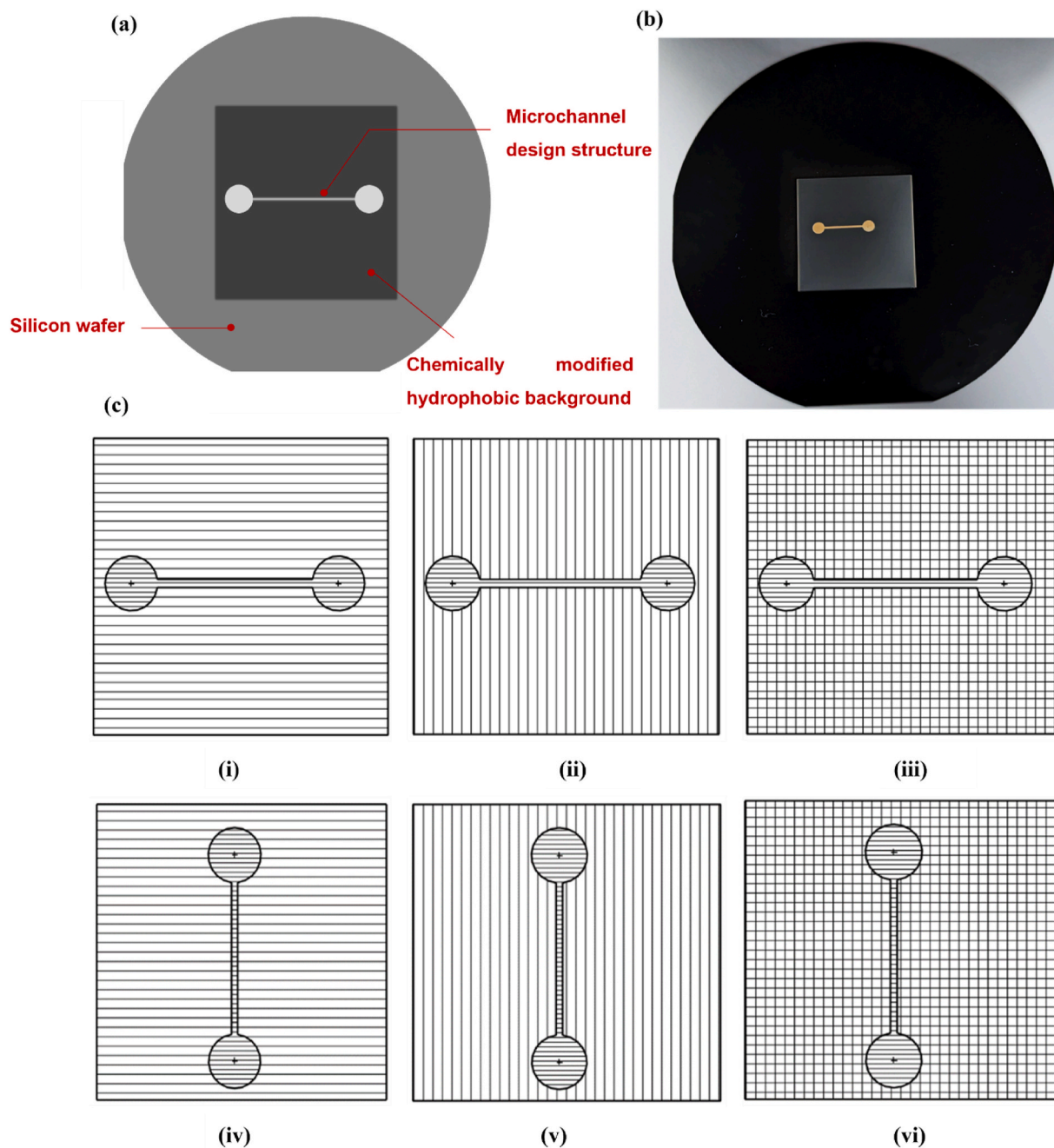


**Fig. 1.** (a) Schematic of the laser textured microchannel structure on post-processed laser pre-machined square background on a 4-inch silicon wafer. (b) Actual image of the laser textured microchannel structure on post-processed laser pre-machined square background on a 4-inch silicon wafer. (c) Scanning line patterns of laser-textured background relative to the microchannel orientation. (i) Horizontal microchannel–scanning lines are parallel to the lines on the background. (ii) Horizontal microchannel–scanning lines are perpendicular to the lines on the background. (iii) Horizontal microchannel on mesh-type background. (iv) Vertical microchannel–scanning lines are parallel to the background lines. (v) Vertical microchannel–scanning lines are perpendicular to the background lines. (vi) Vertical microchannel on mesh-type background.

microchannel structure. Given that the hydrophobic background was also prepared via laser machining, we systematically investigated the effects of its scanning line pattern and the microchannel's orientation relative to the background structure on wicking performance. Our study underscores the transformative potential of laser micromachining in precisely controlling the wicking phenomenon, marking a notable advancement in the field.

## 2. Materials and methods

### 2.1. Fabrication and surface modification of silicon wafers






A series of fabrication steps were performed to investigate the effects of laser-induced surface modifications on silicon wafers. First, 4-inch silicon wafers with  $\langle 100 \rangle$  crystal orientation were ultrasonically cleaned with deionized (DI) water and ethanol. A  $3 \text{ cm} \times 3 \text{ cm}$  square was machined on the silicon substrate using a femtosecond laser machine (A-Series, Oxford Lasers, United Kingdom) wavelength(s) 1028 nm, frequency range 1 kHz–1 MHz, maximum average power 6W at 30 kHz and maximum energy 0.2 mJ at 30 kHz. The laser parameters for this square-shaped background are as follows: laser power of 5 W, scanning speed of 30 mm/s, and scanning line thickness of 80  $\mu\text{m}$ . These parameters were selected to achieve optimal surface texturing while maintaining the integrity of the silicon substrate. Next, the laser-textured surface underwent a chemical post-processing experiment introduced by Tran et al. [20]. This process aimed to shift the wettability of the surface structure from superhydrophilic, induced by laser processing, to hydrophobic.

The design structures, consisting of two inlet and outlet circles (radius = 1.5 mm) connected by a microchannel with a length of 1 cm and a width of 500  $\mu\text{m}$ , were machined on the chemically post-processed hydrophobic background through a second round of laser processing. Fig. 1(a), (b) illustrate the design of the proposed laser-fabricated microstructure.

As the first step of the study, five horizontally oriented microchannel samples, with scanning lines parallel to those of the background (Fig. 1 (c)(i)), were tested. These samples were subjected to variable laser parameters, including laser power, scanning speed, type of scanning lines, and rounds of machining. All the tested samples and their design features are listed in Table 1.

In the second stage, six different samples were designed to investigate the effects of microchannel's orientation (horizontal/vertical) followed by their scanning lines' orientation relative to the background with different laser scanning line patterns, Fig. 1(c). The first category consists of horizontal structures on a hydrophobic background with the

**Table 1**  
Different samples with different laser parameters.

Sample Number	Laser Parameter		Type of Scanning Lines	Number of Laser Passes	Scanning Line Thickness ( $\mu\text{m}$ )
	Laser Speed (mm/s)	Laser Power (W)			
1	30	3	Linear 	1	8
2	4	3	Linear 	1	8
3	30	5	Linear 	1	8
4	30	3	Spiral 	1	8
5	30	3	Linear 	2	8

following scanning line patterns: 1) lines parallel to those of the microchannel, 2) lines perpendicular to the microchannel, and 3) a mesh structure combining both horizontal and vertical lines. These conditions were also examined for the vertical orientation of the channel.

### 2.2. Analysis of wicking behavior

To analyze the wicking behavior of the flow through the microchannel, we utilized a setup consisting of an upright microscope (Nikon SMZ 745T, Japan), a camera (Dino-lite digital microscope camera) mounted on the microscope, and a syringe pump, Fig. 2. The sample was placed under the microscope, and the lighting was adjusted to optimize the experimental conditions. A 5- $\mu\text{l}$  droplet was gently applied to the inlet circle via the syringe pump. The camera recorded the entire process of water flow through the channel. The captured videos were then further processed for quantitative data.

### 2.3. Surface characterization and analysis techniques

We conducted a series of tests at different stages to comprehensively characterize the samples' surface morphology and chemical composition. The surface morphology of the laser-machined microstructures was analyzed using a scanning electron microscope (SEM) (Apreo 2S, Thermo Scientific, United States). The SEM's energy dispersive spectroscopy (EDS) function was employed to detect the chemical composition of the surface structures. The resultant structures' dimensions and average surface roughness (Ra) were evaluated using a 3D laser scanning microscope (LEXT 5100, Olympus, Japan). Water contact angle (CA) values of droplets on the laser-machined structures were measured using an optical tensiometer (Theta Flex, Biolin Scientific, Finland).

## 3. Results and discussion

### 3.1. Surface morphology and chemical composition of laser-machined microchannels

This section details the surface morphology and chemical composition of the laser-machined microstructures, which are critical for understanding their wettability and subsequent fluid dynamics within the microchannels. The morphology of the laser-machined structures was characterized using SEM (Fig. 3(a–f)) and the laser scanning microscope (Fig. 3(g–i)). The SEM images provide detailed topographical features of the microchannels, while the laser microscope offers complementary three-dimensional views of the surface. Fig. 3(a–f) present the SEM images of the laser-machined horizontal microchannel structures on a square-shaped hydrophobic background. These images illustrate the intended wicking region. Images were taken for background surface designs with different scanning line patterns, where the lines on the background are clearly visible.

The laser parameters used for this microchannel align with those specified for sample 1 in Table 1. The SEM images reveal a distinct array of micro- and nano-scale protrusions on the surface of the microchannel. During laser machining, the generated heat causes molten material to splash and resolidify, forming these protrusions. Created through laser ablation on the hydrophobic background, these features contribute to surface porosity. The randomly distributed porous micro/nano-structures play a critical role in enhancing the superhydrophilic and wicking properties of the microchannels [21].

EDS analysis was conducted to evaluate the elemental composition of the sample at various stages of processing, Fig. 4(a–d). The EDS data was collected at four stages: (i) pristine silicon substrate, (ii) laser-textured square background immediately after laser machining, (iii) after chemical post-processing, and (iv) after the second round of laser texturing on the chemically modified hydrophobic surface.

Laser machining in air is a high-energy process where silicon reacts with atmospheric oxygen, leading to the formation of silicon oxide on

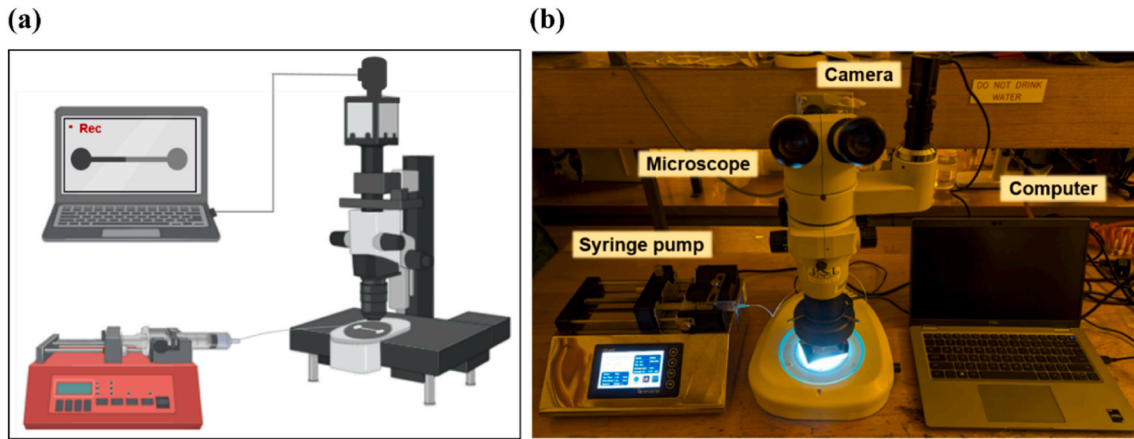


Fig. 2. (a) Schematic illustration of the experimental setup for wicking analysis in laser-machined open microchannels. Created in <https://BioRender.com> (b) Actual image of the setup of the experiment.

the surface of the structure [22]. The increased oxygen content enhances the hydrophilic nature of the silicon surface, which significantly contributes to the super-wicking behavior observed in the laser-textured samples. Elemental composition analysis before and after laser processing shows an increase in the oxygen content after laser machining, which is associated with reactions occurring during the process and the subsequent formation of silicon oxide on the sample.

Following chemical post-processing, the initially superhydrophilic, high-energy laser-textured surface of the square background transitions to a low-energy hydrophobic state. The EDS analysis of chemically post-processed samples reveals a decrease in oxygen content on the square background, Fig. 4(c). This reduction is attributed to the chemical reactions during the processing steps, which effectively altered the surface chemistry.

The EDS analysis of the laser-machined microchannel highlights notable differences in elemental composition, particularly in oxygen content, Fig. 4(d). These variations reflect the complex interactions between laser machining and chemical modifications.

### 3.2. Mechanism of wicking

As previously discussed, the laser machining process significantly alters the silicon surface, transforming the smooth, pristine silicon wafer into a porous, permeable structure [21]. This newly generated porous texture is a key factor in facilitating the wicking phenomenon on the substrate. The primary driving force behind the wickability in these microchannels is the capillary pressure difference. According to the Laplace-Young equation, the capillary pressure difference ( $\Delta P_{cap}$ ) is defined as [23]:

$$\Delta P_{cap} = \frac{2\sigma \cos \theta}{r_p} \quad (1)$$

where  $\sigma$  (N/m),  $\theta$  ( $^\circ$ ) and  $r_p$  (m) are the surface tension, contact angle, and capillary pore radius, respectively.

The capillary pressure difference can be expressed as the sum of viscous friction, gravity, and evaporation effects, contributing to the momentum balance [23]:

$$\frac{2\sigma \cos \theta}{r_p} = \frac{\varphi \mu x v}{k} + \frac{m \mu}{2d_{film} \rho K} x^2 + \rho g h \quad (2)$$

Since the tested samples are positioned horizontally under the microscope (Fig. 2), the effect of gravity is negligible. Additionally, as liquid transport occurs quite rapidly, evaporation of the tested liquid is not a factor. Thus, the equation can be simplified to:

$$\frac{2\sigma \cos \theta}{r_p} = \frac{\varphi \mu x v}{k} \quad (3)$$

$$\frac{dx}{dt} = \frac{2\sigma k \cos \theta}{r_p \varphi \mu x} \quad (4)$$

Capillary filling time can be calculated by integrating with respect to channel length.

$$t = \int_0^x \frac{r_p \varphi \mu x}{2\sigma k \cos \theta} dx \quad (5)$$

The above relation can be rewritten as follows, which is renowned as the Lucas-Washburn equation:

$$x^2 = \frac{4\sigma k \cos \theta}{\mu r_p \varphi} t \quad (6)$$

where  $x$  (m) is the capillary distance travelled by the fluid through the wicking medium,  $k$  ( $m^2$ ) is the permeability function,  $\mu$  (Pa.s) is the liquid viscosity,  $\varphi$  is the porosity factor of the structure and  $t$  is the time.

Equation (6) can be further simplified to  $x^2 = Dt$ , where  $D = \frac{4\sigma k \cos \theta}{\mu r_p \varphi}$  represents the capillary performance parameter. Like the diffusion coefficient, this parameter determines the rate at which fluid traverses the channel.

Based on these relationships, the wicking performance intrinsically depends on both the fluid characteristics and surface properties. In this study, water was chosen as the working liquid in all cases.

### 3.3. Role of laser machining in wicking dynamics

#### 3.3.1. Effect of laser parameters on wicking dynamics of horizontally oriented microchannel

Following two distinct laser machining processes, first, to create a square-shaped hydrophobic background and second, to fabricate the microchannel structure, we observed a pronounced super-wicking phenomenon within the microchannel. When a 5  $\mu$ l water droplet was applied to the inlet circle, water flowed through the microchannel, constrained by the surrounding hydrophobic region, with no lateral spreading. The microchannel demonstrated super hydrophilic properties, while the background remained hydrophobic, keeping the applied droplet in a stable, spherical shape.

Five case studies were conducted to understand how varying laser parameters influence wicking behavior in microchannel structures. Each case analyzed wicking performance in horizontally oriented microchannel under conditions illustrated in Fig. 1(c)(i). Table 1 summarizes the samples' characteristics and the corresponding laser parameters.



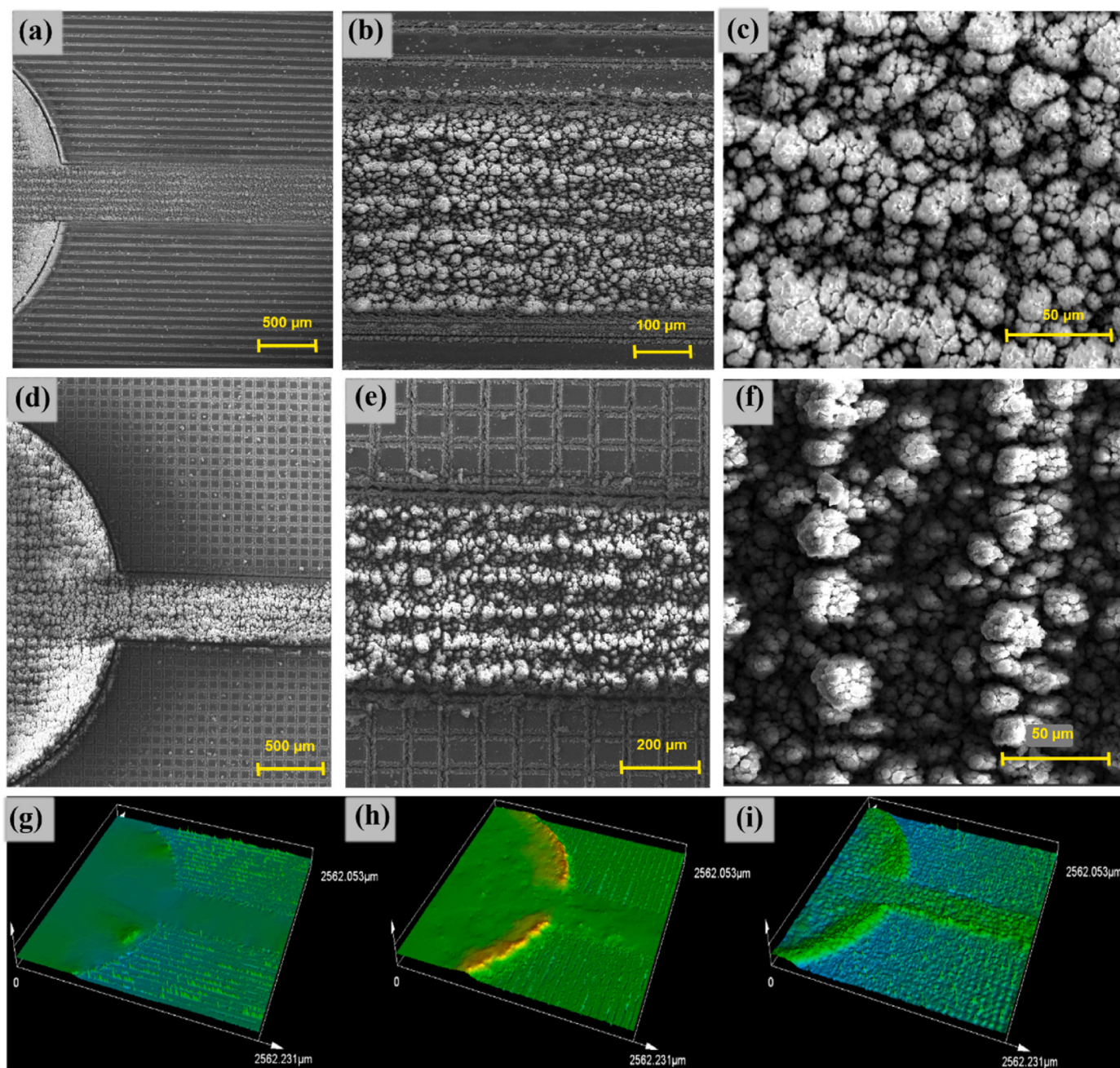


**Fig. 3.** SEM images of laser-machined microchannel on hydrophobic background. (a–c) Horizontal microchannel with scanning lines parallel to the background's lines. (d–f) Horizontal microchannel on hydrophobic background with mesh patterns. Laser microscopy images of (g) horizontal microchannel on background with parallel scanning lines to microchannel's lines. (h) Horizontal microchannel on background with perpendicular lines relative to the microchannel scanning lines. (i) A horizontal microchannel on the background with a mesh pattern.

**Fig. 5** depicts all the meniscus  $x$  position versus time graphs of the tested samples.

**3.3.1.1. Laser scanning speed.** **Fig. 5(a)** shows the data plot of the capillary dynamics for sample 1, with the water spreading duration recorded 4 s. Snapshots of the water propagation through the microchannel at different time intervals ( $t = 0s$ ,  $t = 1s$ ,  $t = 2s$ ,  $t = 3s$ ,  $t = 4s$ ) are provided in **Fig. 5(b)**. Capillary flow progresses through several distinct stages [17,24]. The first stage is the acceleration phase, where the spreading distance of the water is proportional to the square of time ( $x \propto t^2$ ), and the velocity peaks [17]. During this phase, the fluid in sample 1 reaches an initial flow velocity of approximately  $2000 \mu\text{m/s}$  (refer to the velocity–time graph in **Fig. 5(a)**). After the acceleration

phase, the flow transitions into an inertial (or quasi-linear) mode; the distance travelled by the fluid changes linearly with time ( $x \propto t$ ), and the velocity remains constant [17]. This stage lasts for around 0.2 s for this sample. The fluid then enters the Washburn regime, where the spreading distance is proportional to the square root of time ( $x \propto t^{1/2}$ ). **Fig. 5(c)** presents the comparison between experimental  $x \propto t^{1/2}$  data plot for sample 1 with the theoretical values based on Washburn theory.

To explore how laser scanning speed affects the wicking dynamics of microchannels, the scanning speed was varied from 30 mm/s to 4 mm/s **Fig. 5(d)** displays the fluid travel distance over time for samples 1 and 2, which were subjected to various laser scanning speeds. The results indicated that decreasing the laser scanning speed from 30 mm/s to 4 mm/s reduces the flow velocity over time. As shown in the graph, it

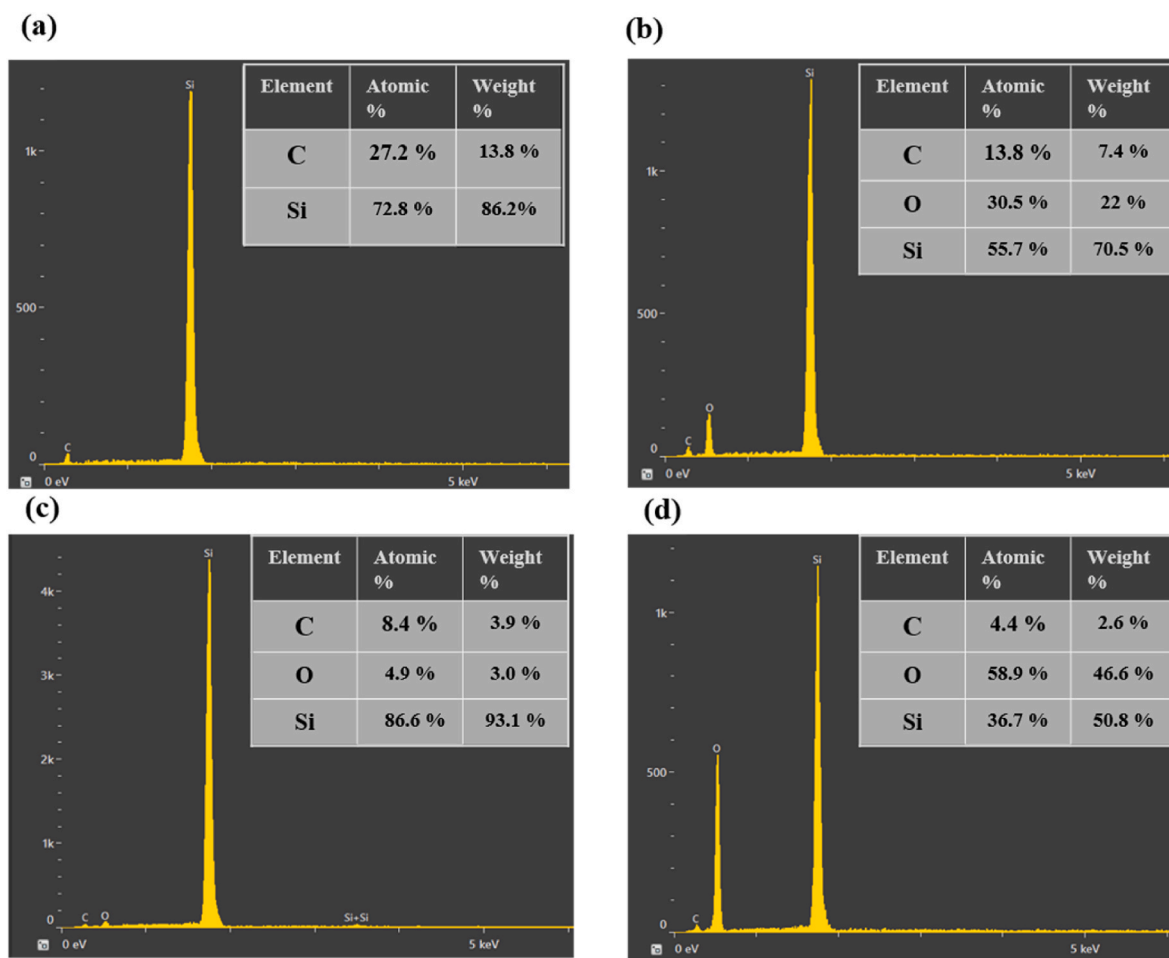


Fig. 4. EDS analysis of (a) Pristine silicon wafer (b) Fresh laser-machined background. (c) Post-processed background. (d) Laser-textured microchannel on hydrophobic background.

takes only 4 s for the fluid to traverse the 1 cm length of the microchannel in sample 1, whereas fluid in sample 2 requires 12.5 s to cover the same distance.

The laser scanning speed directly influences the duration of laser-surface interaction. At a scanning speed of 4 mm/s, the laser beam spends significantly more time on the engraving area compared to a speed of 30 mm/s. As a result, the heat generated has a more pronounced effect on the sample at the lower scanning speed. This phenomenon significantly influences the surface properties and subsequently the wicking dynamics of the sample. The wetting property of surfaces was characterized by analyzing the water contact angle, which is determined by surface chemistry and roughness.

The initial contact angle of a 3- $\mu$ L water droplet on the channel surface was measured:  $30^\circ \pm 2$  for sample 1, and  $56^\circ \pm 3$  for sample 2. The observed difference in contact angles between these two samples is attributed to the distinct surface properties induced by laser ablation. Specifically, the smaller water droplet contact angle on sample 1 indicates a higher level of hydrophilicity, resulting in superior wicking performance as compared to sample 2.

**3.3.1.2. Laser power and scanning line pattern.** The effects of laser power and scanning line pattern on the wicking behavior of the microchannel were also investigated. Laser power represents the energy delivered by each laser spot, with higher power resulting in more intense energy emission onto the sample. Fig. 5(e) demonstrates that increasing laser power from 3W (sample 1) to 5W (sample 3) results in a decrease in the capillary flow rate.

A sample with a spiral-shaped scanning line pattern was fabricated to evaluate the impact of different laser scanning line patterns on microchannel wickability, as shown in Table 1 (sample 4). The meniscus  $x$  position versus time graphs for the linear (sample 1) and spiral (sample 4) patterns (Fig. 5(e)) show only slight differences. This is because the scanning line pattern in the channel section of the microstructures is the same. The primary difference between these designs lies in the engraving line pattern in the inlet and outlet circles, indicating that the inlet's scanning line pattern minimally influences the wicking behavior. However, the shape of the scanning lines alters the flow pattern, leading to a different fluid flow shape in the outlet circle compared to the linear type.

**3.3.1.3. Multiple laser passes.** In the final step of this study, the effect of multiple laser passes was analyzed. A sample was fabricated with two rounds of laser passes, and the resulting distance versus time graph is shown in Fig. 5(f) (sample 5). The figure indicates that increasing the number of laser passes reduces the water flow rate in the microchannel. For instance, the 1 cm microchannel was traversed in 4 s by the applied water droplet on the sample with 1 round of laser pass (sample 1), whereas it took 6.4 s for the sample with two rounds of machining (sample 5). Two rounds of laser passes altered the microchannel's surface properties, increasing surface roughness and changing the amount of element oxide due to repeated machining.

We non-dimensionalize the relationships to simplify the resulting spreading distance versus time graphs. From the Washburn equation, Equation (6), the non-dimensional parameter is defined as:

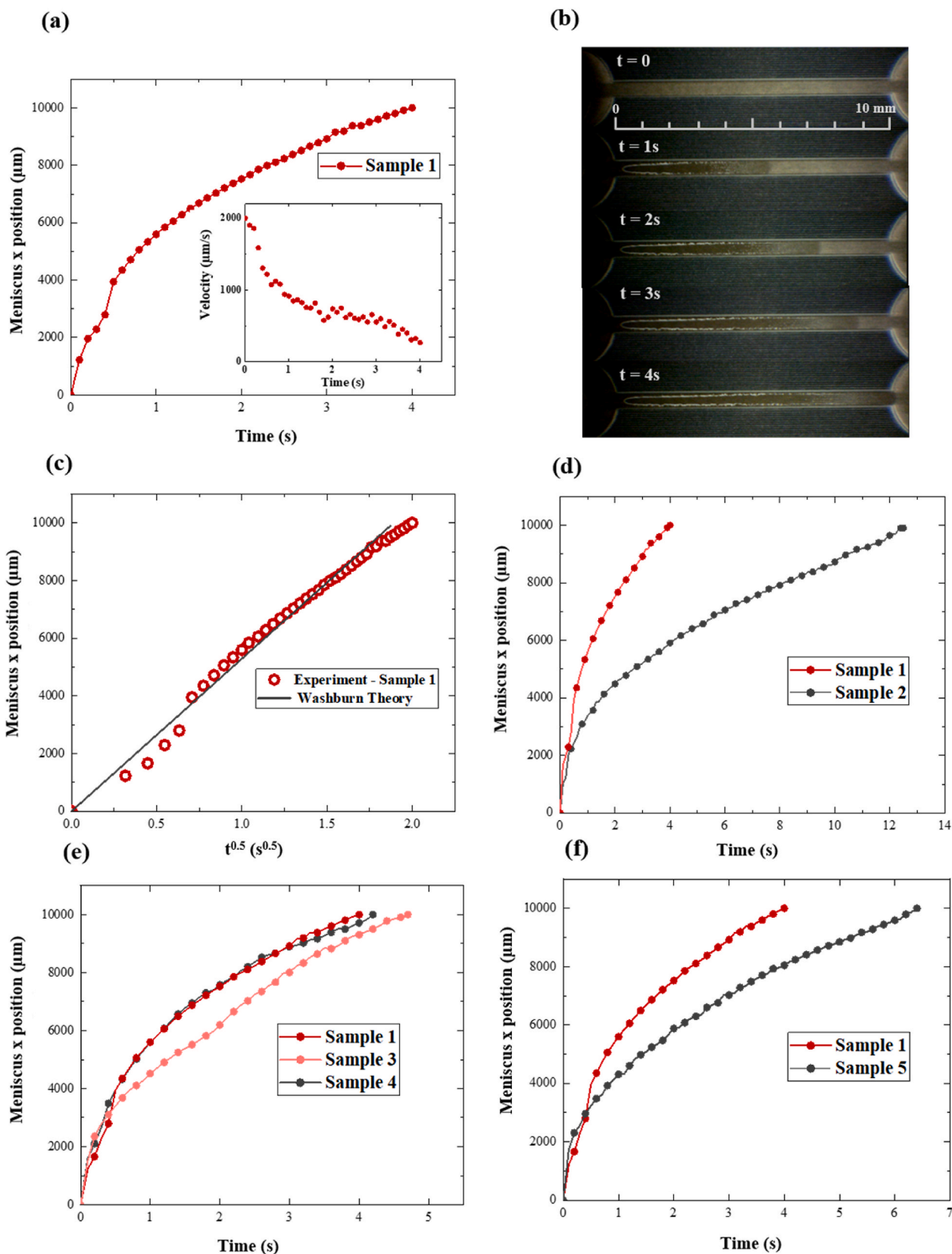


Fig. 5. Wicking performance analysis. (a) Meniscus x position versus time and velocity versus time graphs for sample 1. (b) Snapshots of water spreading in the microchannel (at  $t = 0$ ,  $t = 1$  s,  $t = 2$  s,  $t = 3$  s,  $t = 4$  s). (c) Meniscus x position versus  $t^{1/2}$  graphs of experiment (sample 1) and Washburn theory. (d) Meniscus x position versus  $t$  graph for samples 1 and 2. (Effect of laser scanning speed) (e) Meniscus x position vs time graph for samples 1, 3 and 4. (Effect of laser power and scanning line pattern). (f) Meniscus x position vs time graph for samples 1 and 5. (Effect of number of laser passes).



$$K = \frac{k \cos \theta}{r_p \phi} \quad (7)$$

Therefore, non-dimensionalized  $x^*$  and  $t^*$  can be calculated as follows:

$$x^* = \frac{x}{K}, t^* = \frac{t \cdot D}{K^2} \quad (8)$$

Fig. 6 shows the  $x^{*2} - t^*$  graphs for all 5 samples.

The resulting plot reveals that the general pattern of the  $x^{*2} - t^*$  graphs for these five samples is linear. Differences among these data sets arise from factors related to surface properties, which reflected in the calculated parameters.

The tested samples exhibit various modes of capillary-induced fluid flow, characterized by distinct surface characteristics resulted from different laser machining conditions. These characteristics include average surface roughness (Ra,  $\mu\text{m}$ ), capillary performance factor (D,  $\text{m}^2/\text{s}$ ), and water contact angle ( $^\circ$ ). Ra, D and initial water contact angle were measured for each case and are summarized in Table 2. Additionally, the contact angle evolution of a 3- $\mu\text{L}$  water droplet, from initial placement to complete spreading on the channel surface, was recorded for each sample (Fig. 7(a)), highlighting variations in wetting dynamics. These parameters indicate each surface structure's hydrophilicity level and, consequently, its wickability. Higher D values, combined with lower initial contact angles and shorter droplet spreading times, suggest enhanced wickability of the microchannel structures.

Table 2 shows that sample 2, which demonstrates the weakest wickability, has the lowest D parameter and the highest initial contact angle among the cases. In contrast, sample 1, which exhibits the best wicking performance, has the highest D value and the lowest initial contact angle. In addition, a correlation exists between surface roughness and the capillary performance factor. As shown in Table 2, samples with lower average roughness values exhibit better wicking performance, indicated by higher D values. Fig. 7(b) further illustrates this relationship, showing that Ra is inversely related to D: as surface roughness increases, the capillary performance factor—and thus, wicking dynamics—decrease. This inverse relationship suggests that the distribution and inherent characteristics of the generated roughness act as a hindrance, where increased roughness slows the water flow rate.

### 3.3.2. Effect of laser engraving line pattern of hydrophobic background and microchannel orientation on wicking dynamics

The primary purpose of designing a hydrophobic background was to restrict the water flow within the borders defined by the microchannel

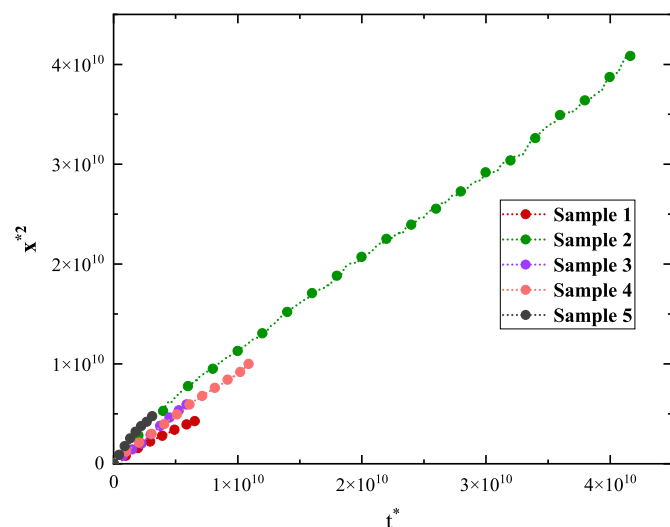


Fig. 6. Non-dimensional  $x^{*2} - t^*$  graphs for 5 samples of horizontal microchannels.

Table 2  
Surface characteristic parameters.

Sample Number	Initial contact angle (deg)	Ra ( $\mu\text{m}$ )	D ( $\text{m}^2/\text{s}$ )
Sample 1	$30 \pm 2$	1.347	$2.8 \times 10^{-5}$
Sample 2	$56 \pm 3$	9.54	$6.6 \times 10^{-6}$
Sample 3	$33 \pm 2$	1.768	$2.14 \times 10^{-5}$
Sample 4	$30 \pm 2$	1.525	$2.6 \times 10^{-5}$
Sample 5	$35 \pm 1$	3.51	$1.68 \times 10^{-5}$

walls. However, further analysis reveals that the background pattern also plays a significant role in controlling the wicking dynamics within the microchannel. This background not only serves as a mechanism for lateral water flow control but also introduces a novel approach for manipulating wicking behavior. Various strategies have been explored to control wicking, including modifications to the wicking region, such as altering the structure's shape or adjusting laser parameters, as discussed in the previous section of the current study. Additionally, chemical surface treatments can be employed to modify wickability.

In this section, we present another factor to manipulate the wicking dynamics, i.e., the characteristics of the laser-textured hydrophobic background surface. Three distinct cases were investigated, as illustrated in Fig. 1(c).

- **Parallel Scanning Lines:** The scanning lines of the microchannel run parallel to those on the hydrophobic background.
- **Perpendicular Scanning Lines:** The scanning lines of the microchannel are oriented perpendicular to the lines of the background.
- **Mesh Pattern:** The scanning lines of the hydrophobic background create a mesh pattern, combining both vertical and horizontal lines.

This section reports on the effects of various hydrophobic background patterns on the wicking dynamics of the samples. These effects were analyzed for two configurations: microchannels oriented horizontally and vertically relative to the square background structure. Note that the laser parameters for all the tested samples of this section match those of sample 1 in Table 1.

3.3.2.1. *Horizontal orientation.* The orientation of the microchannel structure dictates the engraving line style and the corresponding laser scanning pattern. Fig. 8 illustrates the differences in the scanning paths between horizontally and vertically oriented microchannels. These orientations influence the beam motion during the process and the duration of laser exposure on the surface, affecting the microstructure formation.

Fig. 9(a) presents the meniscus  $x$  position versus time graphs for horizontally oriented channels on backgrounds with different laser scanning line patterns. According to this graph, among the three configurations of horizontally oriented channels, the first type—where the scanning lines are parallel to the lines of the hydrophobic background—provides the best wicking performance in terms of the time required for the fluid to traverse the 1 cm microchannel. This path was travelled in 4 s for parallel and 10.8 s for perpendicular style samples. For the mesh pattern of the hydrophobic background, the water only partially wets the surface of the microchannel, failing to pass beyond 4 mm.

3.3.2.2. *Vertical orientation.* Next, we changed the microchannel orientation from horizontal to vertical. If rotated  $90^\circ$ , the scanning lines on the surface of these microchannels were aligned differently from those on horizontal channels, Fig. 8(b). This shift in the laser engraving line pattern leads to distinct wicking dynamics. Fig. 9(c and d) presents velocity-over-time graphs for both orientations, each having the same laser scanning line design (with channel lines parallel to those on the background). The vertical microchannel exhibits higher velocity magnitudes compared to the horizontal one. Specifically, the initial flow velocity reaches  $3108 \mu\text{m}/\text{s}$  in the vertical microchannel, whereas it



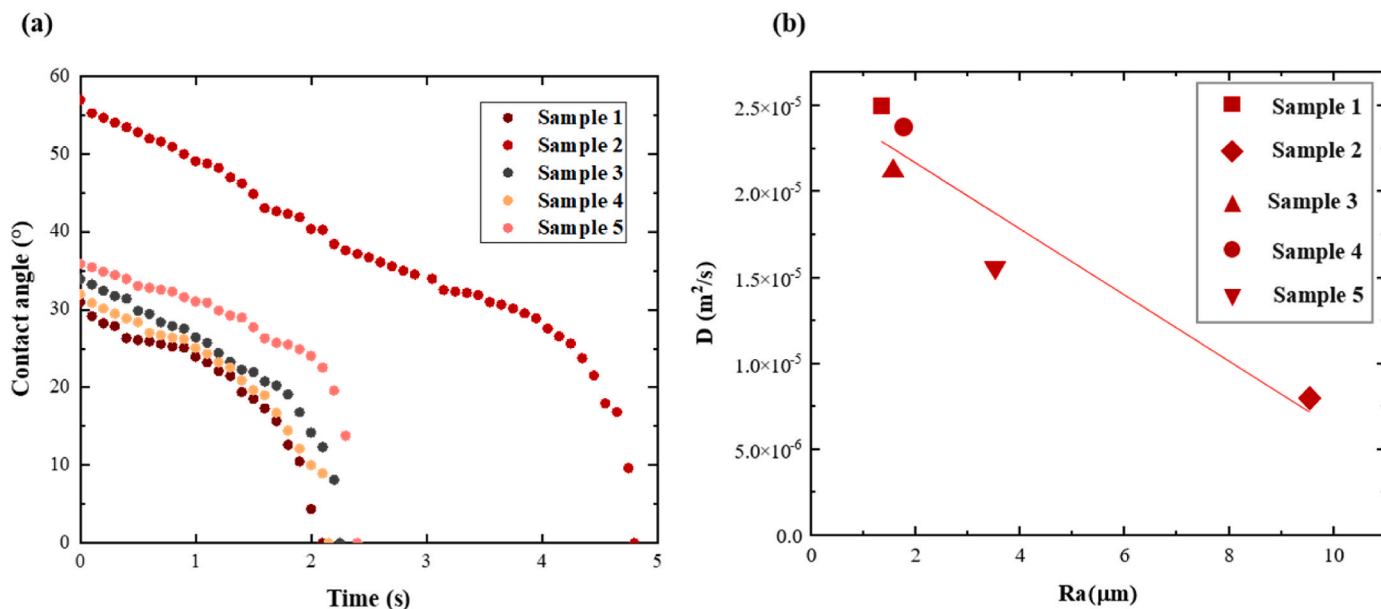


Fig. 7. (a) Water contact angle evolution of droplet on the channel section of the tested samples (b) D - Ra trend for the tested samples. The sample numbers correspond to those listed in Table 1.

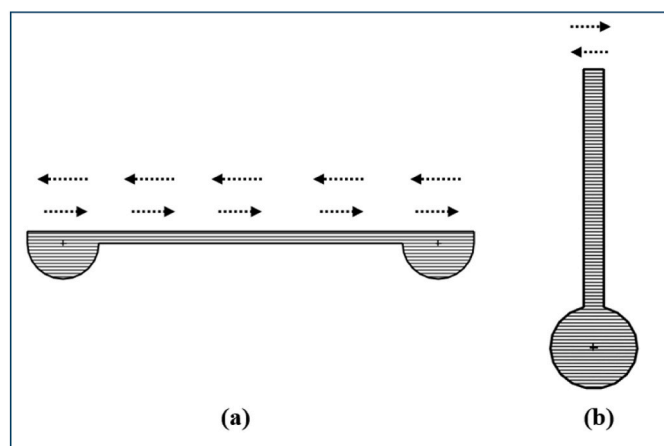


Fig. 8. Schematic of laser beam motion direction for microchannels in (a) Horizontal (b) Vertical orientation.

reaches 2000  $\mu\text{m/s}$  in the horizontally orientated channel.

Fig. 9(b) shows that all three vertically oriented microchannels on hydrophobic background with different scanning line styles exhibit faster wicking than their horizontal counterparts, most notably on the mesh-patterned background. In the horizontal position, water in channel on the mesh background fails to traverse the microchannel fully. Meanwhile, in the vertical orientation, water completes the 1-cm path in just 2.2 s. Among the three vertical configurations, the microchannel on the mesh-patterned background exhibits the best performance, with a complete water spreading time of 2.2 s. This is followed by the microchannel on the background with perpendicular scanning line alignment relative to the channel (2.5 s) and the parallel alignment (3.4 s).

The surface characteristics of horizontal and vertical microchannels, with scanning lines parallel to the background lines, were analyzed using contact angle measurements. Fig. 10(a) and (b) depict the droplet behavior on the surface of each sample. In the horizontal orientation, the droplet retains its spherical shape after detachment from the dispenser. Conversely, the droplet spreads immediately upon detachment in the vertical orientation, showing no spherical form. This fast droplet spreading reflects a higher degree of superhydrophilicity in the vertical

microchannels than the horizontal ones.

The observed differences highlight variations in the inherent surface properties of the two samples, as reflected in the droplet behavior on each. Both surface chemistry and topography (roughness) determine the mode of surface wetting. In this case, the chemical composition of the two structures is identical, as both channels were fabricated on the same substrate with equivalent properties. The key difference, however, lies in the surface morphological features.

Fig. 10 (c)–(f) present SEM images of these microchannels, highlighting differences in surface morphology and physical properties of laser-generated surface roughness between the two orientations. The SEM images of the horizontally oriented microchannel (Fig. 10(c) and (d)) show a surface with loosely arranged micro bumps in an array-like pattern. In contrast, the vertical microchannel (Fig. 10(e) and (f)) exhibit a more densely packed structure characterized by a cauliflower-like morphology with a crust-like layer containing visible microcracks.

Surface roughness (Ra) and the capillary performance parameter (D) were measured for all samples. Fig. 11(a) and (b) illustrate the relationship between D and Ra for both horizontal and vertical microchannels. For horizontal samples (Fig. 11(a)), an inverse relationship is observed, where increased roughness results in lower D values. This suggests that greater roughness correlates with a reduced capillary flow rate in horizontally oriented microchannels, a trend consistent with the five samples discussed in the previous section.

In contrast, the D-Ra relationship for vertical microchannels (Fig. 11 (b)) shows a direct correlation, with increased roughness enhancing wicking dynamics. This trend is further highlighted in samples subjected to multiple laser passes: two laser passes on horizontally oriented microchannels result in increased roughness and a slower flow rate (Fig. 11(c)). However, for vertical microchannels, two laser passes, despite increasing roughness, yield a higher flow rate than a single pass (Fig. 11(d)).

The contrasting behaviors of vertical and horizontal microchannels highlight the impact of surface roughness on capillary flow. Rough surfaces can create energy barriers that affect liquid movement. Depending on their nature and distribution, these barriers can either facilitate or hinder wicking. Increased roughness may pin the water contact line, slowing or stopping the flow [25]. However, it can also enhance wicking by increasing contact surface area and improving liquid-surface contact points, thereby enhancing capillary action [26].

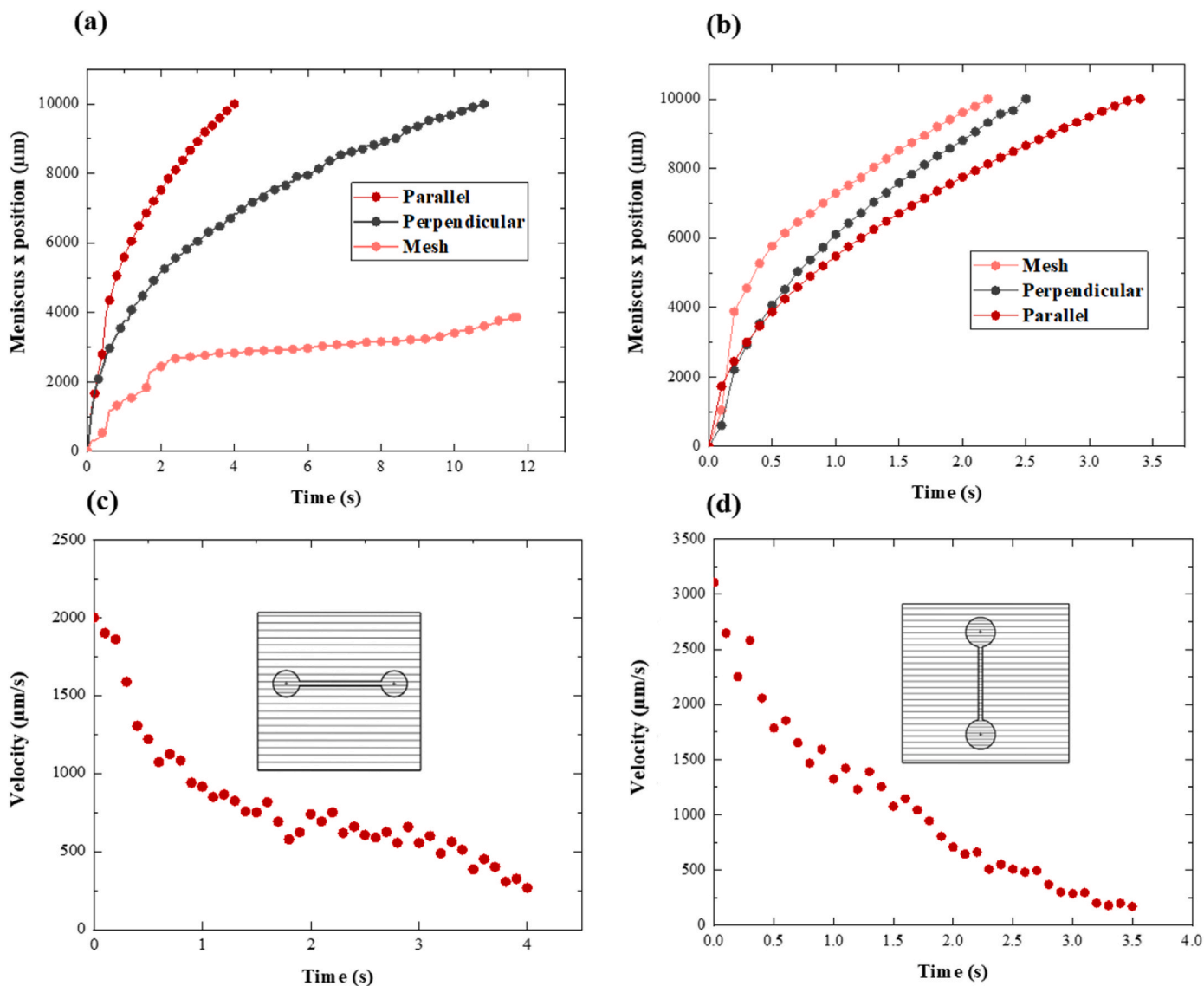


Fig. 9. Meniscus x position versus time graphs of (a) Horizontal (b) Vertical microchannels on hydrophobic background surfaces with different scanning line patterns. Velocity versus time graphs of (c) Horizontal (d) Vertical microchannels with scanning lines parallel to the background's lines.

This dual influence of roughness is apparent in the varied wicking performance of samples with different orientations, attributable to differences in the morphology and distribution of the micro/nanostructures generated by laser treatment (see Fig. 10(d)–(f)).

### 3.4. Role of laser machining in water front meniscus shape

The meniscus shape of the water-front line reflects the surface characteristics of the microchannels. By comparing the meniscus shapes for vertical and horizontal microchannels, both processed under identical laser conditions (including laser parameters and scanning line orientation relative to the background), differences in surface properties are observed. Fig. 10(g, h) illustrate the meniscus shapes for horizontal and vertical microchannels, with scanning lines parallel to those on the background.

The vertical microchannel, which exhibits superior wicking performance, possesses a concave meniscus. This concavity suggests that the adhesion between the liquid and the microchannel walls is stronger than the cohesion among water molecules. Conversely, the horizontally oriented microchannel displays a convex meniscus. The disparity in meniscus shapes is attributed to variations in laser processing between

the two orientations, resulting in distinct wetting patterns on the machined surfaces.

Laser machining typically induces a superhydrophilic wetting mode on the channel surface; however, the hydrophilicity level may vary across the surface. This variation arises from specific patterns of micro- and nano-scale protrusions generated by the laser. SEM images in Fig. 10 (c) and (e) highlight these structural differences for the two cases of horizontal and vertical microchannels. Closer examination of the vertical microchannel section reveals a more pronounced aggregation of silicon oxide with a dense distribution along the channel walls. This denser distribution likely contributes to the concave meniscus shape observed in the water front, suggesting a higher degree of hydrophilicity on the channel side walls, which promotes water attraction and shapes the meniscus morphology.

### 3.5. Role of laser machining in wicking durability

The metal surface initially becomes superhydrophilic after laser machining, exhibiting excellent wickability. However, this property degrades over time when exposed to ambient air. Despite the unchanged morphology of the laser-engineered structure, the transition from

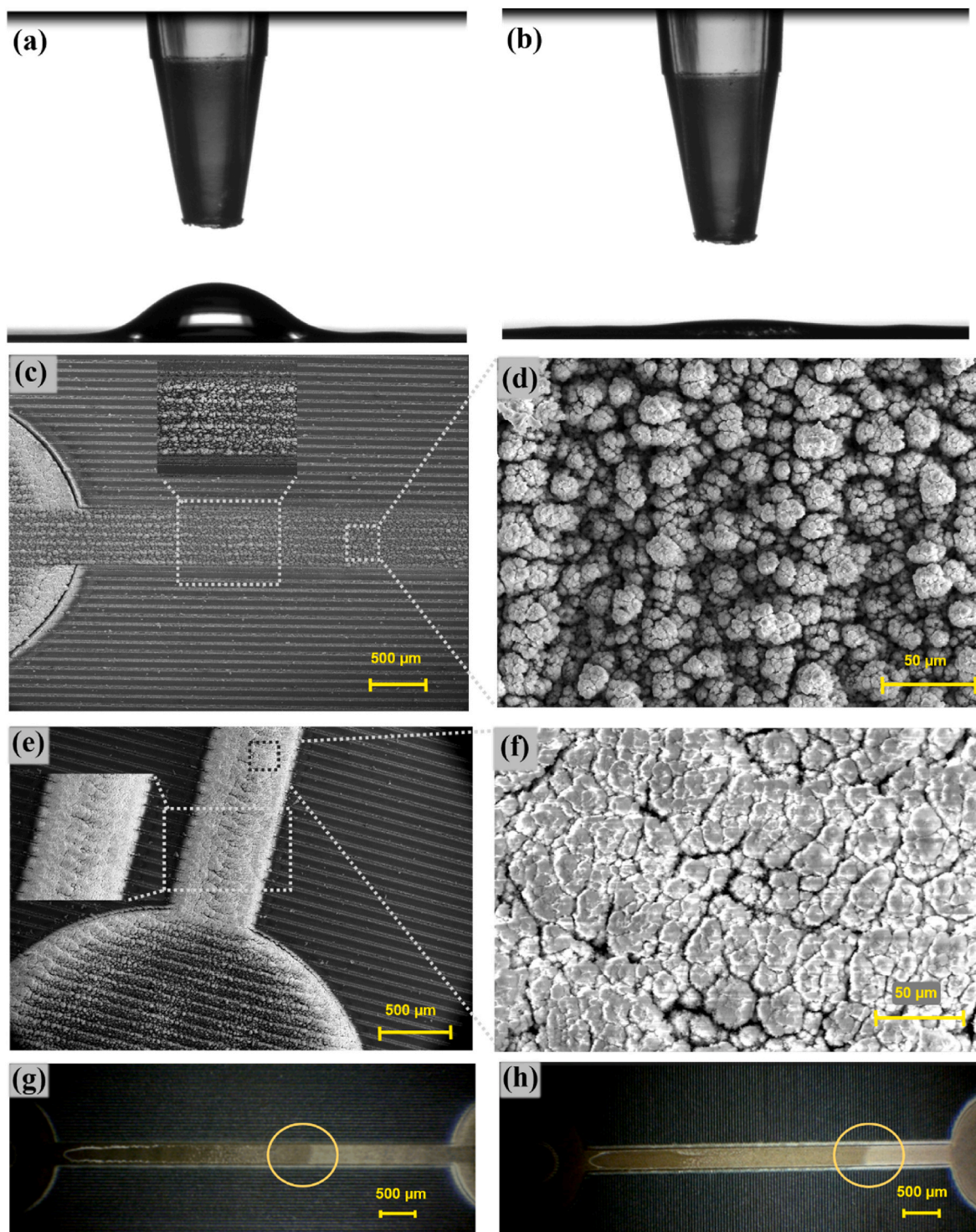


**Fig. 10.** Water droplet contact angle measurement test on (a) Horizontal (b) Vertical microchannels with scanning lines parallel to the lines on the background. SEM images of (c) Horizontal microchannel (d) Close view of the channel section. (e) Vertical microchannel (f) Close view of channel section. Schematic illustration of (g) Convex shape of meniscus of water-front line of the horizontal microchannel. (h) The concave shape of the meniscus of the vertical microchannel.

superhydrophilic to hydrophobic behavior results from changes in surface chemistry: the surface gradually absorbs organic substances from the environment, which diminishes its wickability [22]. Consequently, the high level of wickability achieved by laser machining is not inherently stable and is susceptible to environmental conditions. Wickability durability is crucial for the longevity of the wicking effect. This study demonstrates how laser machining can impact the durability of wicking performance, with wicking durability of microchannels being adjustable

by modifying laser machining conditions.

Among the horizontally oriented microchannels, sample 5—subjected to two laser passes—exhibits the highest durability. Although its initial wicking performance is weaker than that of the single-pass sample (sample 1), it retains this property longer over time. As shown in Fig. 12(a), which presents the meniscus x-position versus time for sample 5 after 15 days, the number of laser passes significantly enhances durability. Notably, all other horizontally oriented samples



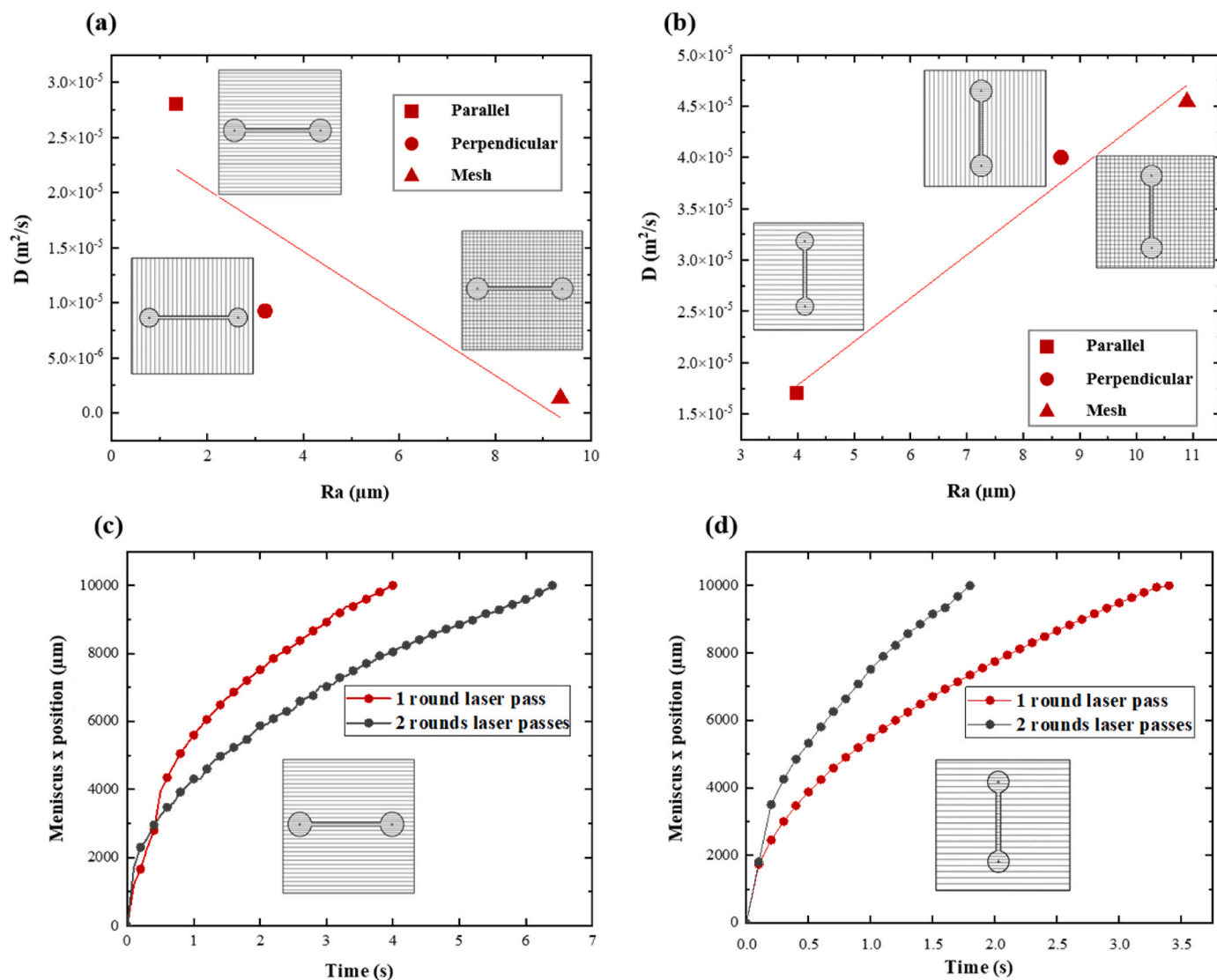


**Fig. 11.** (a) D – Ra trend for horizontal microchannels on different background designs. (b) D- Ra trend for vertical microchannels on different background designs. (c) Meniscus x position versus time graph for horizontal microchannel with one and two rounds laser passes. (d) Meniscus x position versus time graph for vertical microchannel with one and two rounds laser passes.

shifted to a hydrophobic state during this period.

In case of channel orientation, the vertical style exhibits more durable behavior than its horizontal counterpart. Fig. 12(b) illustrates this difference 7 days after laser processing.

The observed differences in wicking longevity among these samples can be attributed to variations in surface properties resulting from the laser machining process. Interestingly, the superior wicking durability of sample 5 compared to sample 1, despite its weaker capillary performance, suggests that surface durability is closely related to roughness physical properties (morphology and arrangement) than to capillary flow performance.

The more durable samples possess higher roughness values. For instance, sample 5, which underwent two rounds of laser machining, has an average roughness of 3.51 μm, compared to 1.347 μm for the single-pass channel. Moreover, when comparing microchannels with identical laser machining conditions but differing orientations, the vertically oriented microchannel demonstrates higher roughness than the horizontal counterpart.

However, high roughness alone is insufficient to ensure wicking durability. The distribution pattern of laser-generated micro- and nanostructures plays a more critical role in maintaining durable wicking

properties. SEM images of samples 1, 5 and the vertically oriented microchannel reveal that samples with greater wicking durability (sample 5 and the vertical microchannel) display tighter, more compact micro/nano structural distribution patterns (Fig. 12(c-e)). As previously discussed, the transition from a laser-induced superhydrophilic to a hydrophobic state is driven by the adsorption of airborne organic compounds. A denser micro/nanostructure arrangement restricts the diffusion of the adsorbed compounds [22], thereby enhancing the stability of the surface wettability.

#### 4. Conclusion

Laser machining has proven to be an effective method for inducing superhydrophilicity and enhancing wicking performance on metal surfaces. Various capillary dynamics can be achieved by modifying the structures' physical and chemical characteristics. This study demonstrates how different laser conditions affect the wicking behavior of microchannels on a chemically modified hydrophobic surface.

The findings reveal that the wettability induced by laser machining varies with the conditions used. The nature and distribution of the generated roughness strongly impact capillary dynamics, either



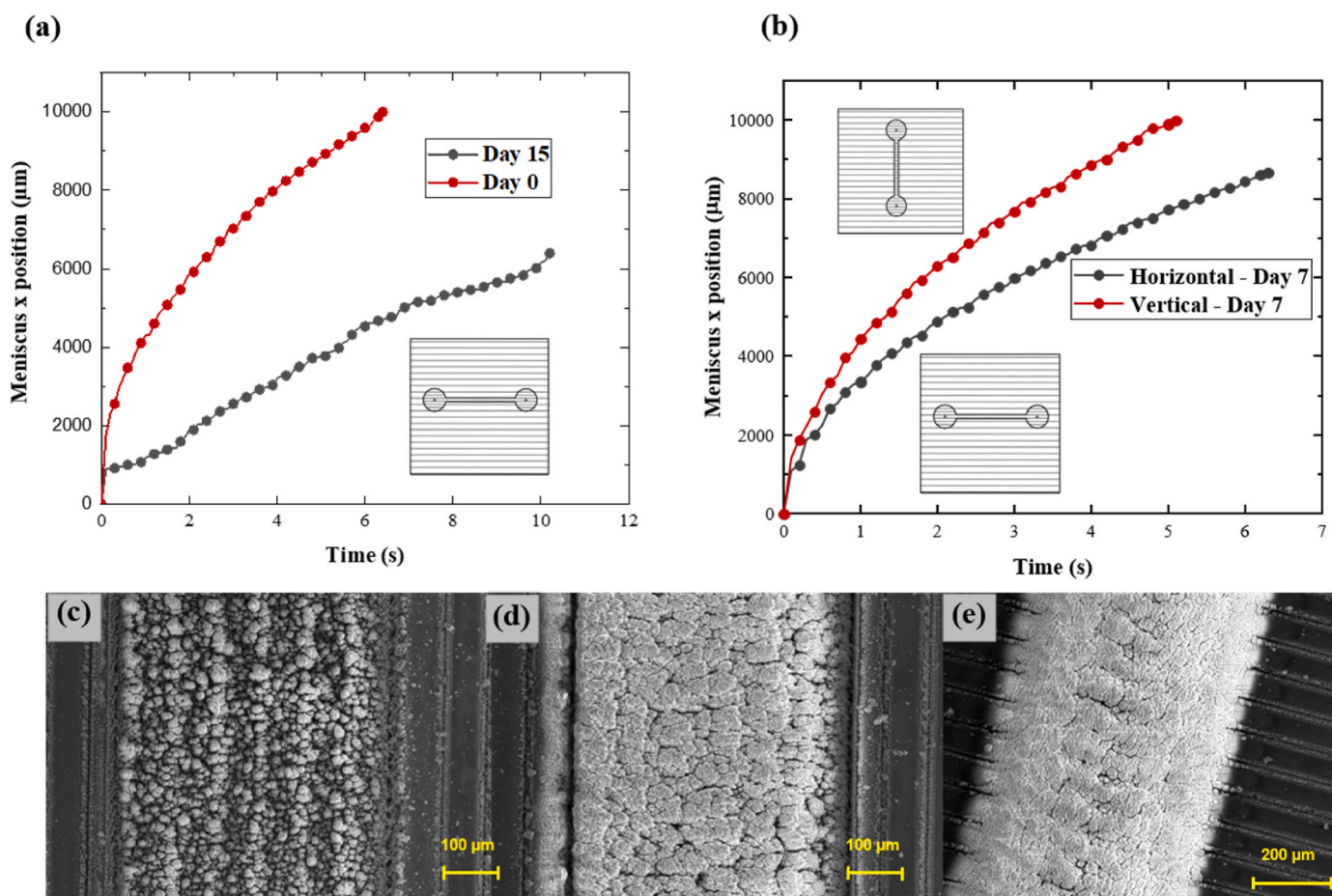


Fig. 12. Meniscus x position versus time graphs for (a) Horizontal microchannel with two laser passes (sample 5) on Day 0 and Day 15. (b) Horizontal and vertical microchannels on Day 7. SEM images of channel section of (c) sample 1 (d) sample 5 (e) vertically oriented microstructure.

enhancing or impeding the flow. For horizontally oriented channels, increased roughness leads to a slower flow rate. In contrast, in vertically oriented microchannels, higher roughness results in a faster water flow rate. For example, among horizontal channels on different background patterns, the fastest flow rate (1 cm in 4 s) was observed in the channel with scanning lines parallel to the background's lines, which also had the lowest roughness value (1.347  $\mu\text{m}$ ) compared to the channel with scanning lines perpendicular to the background's (3.265  $\mu\text{m}$ ) and that on a mesh-patterned background (9.418  $\mu\text{m}$ ). On the other hand, in vertical channels, the roughest case (channel with average roughness of 11.013  $\mu\text{m}$  on mesh-type background) achieved the fastest wicking flow rate, passing 1 cm in just 2.2 s.

Notably, vertical microchannels show greater durability in wicking performance over time compared to horizontal ones, and increasing the number of laser passes improves the surface's resistance to wetting transition. It should be added that surface durability appears to be more closely related to roughness than to wicking dynamic performance, as confirmed by the results from the sample with multiple rounds of machining for horizontally oriented microstructure.

These insights have important implications for applications where precise fluid movement control is crucial, such as in microfluidic devices for biomedical diagnostics, lab-on-a-chip technologies, and advanced material handling systems. Future research should further optimize laser machining parameters to enhance wicking performance and durability in various applications. Investigating the long-term stability of the induced hydrophilic states under different environmental conditions and exploring the potential for integrating these techniques into practical devices will be essential for advancing the field.

#### CRediT authorship contribution statement

**Elham Lori Zoudani:** Writing – review & editing, Writing – original draft, Visualization, Validation, Software, Methodology, Investigation, Data curation. **Nam-Trung Nguyen:** Writing – review & editing, Supervision, Resources, Project administration, Formal analysis, Conceptualization. **Navid Kashaninejad:** Writing – review & editing, Validation, Supervision, Resources, Project administration, Funding acquisition, Formal analysis.

#### Declaration of competing interest

The authors declare that they have no known competing financial interests or personal relationships that could have appeared to influence the work reported in this paper.

#### References

- [1] H.H. Vu, N.-T. Nguyen, N.-K. Nguyen, C.H. Luu, S. Hettiarachchi, N. Kashaninejad, Tunable wettability with stretchable microstructured surfaces, *Adv. Eng. Mater.* 25 (23) (2023) 2300821.
- [2] B.E. Rapp, *Microfluidics: Modeling, Mechanics and Mathematics*, Elsevier, 2022.
- [3] S. Patari, P.S. Mahapatra, Liquid wicking in a paper strip: An experimental and numerical study, *ACS Omega* 5 (36) (2020) 22931–22939.
- [4] A. Samanta, Q. Wang, S.K. Shaw, H. Ding, Roles of chemistry modification for laser textured metal alloys to achieve extreme surface wetting behaviors, *Mater. Des.* 192 (2020) 108744.
- [5] S.A. Khan, V. Ialyshev, V.V. Kim, M. Iqbal, H. Al Harmi, G.S. Boltaev, R.A. Ganeev, A.S. Alnaser, Expedited transition in the wettability response of metal meshes structured by femtosecond laser pulses for oil-water separation, *Front. Chem.* 8 (2020) 768.

- [6] G.U. Kumar, S. Suresh, C.S. Kumar, S. Back, B. Kang, H.J. Lee, A review on the role of laser textured surfaces on boiling heat transfer, *Appl. Therm. Eng.* 174 (2020) 115274.
- [7] Y. Wu, G. Zou, C. Du, Y. Xiao, X. Zhou, R. Geng, H. Yu, C. Lv, L. Liu, Enhanced capillary performance of multiscale ultrathin titanium wicks guided by modified wicking dynamics, *Int. J. Heat Mass Tran.* 221 (2024) 125000.
- [8] M. Ochoa, H. Jiang, R. Rahimi, B. Ziaie, Laser treated glass platform with rapid wicking-driven transport and particle separation capabilities. 2015 28th IEEE International Conference on Micro Electro Mechanical Systems (MEMS), IEEE, 2015, pp. 332–335.
- [9] R. Fang, Z. Li, X. Zhang, X. Zhu, H. Zhang, J. Li, Z. Pan, Z. Huang, C. Yang, J. Zheng, Spreading and drying dynamics of water drop on hot surface of superwicking Ti-6Al-4V alloy material fabricated by femtosecond laser, *Nanomaterials* 11 (4) (2021) 899.
- [10] E. Stratakis, J. Bonse, J. Heitz, J. Siegel, G. Tsibidis, E. Skoulas, A. Papadopoulos, A. Mimidis, A.-C. Joel, P. Comanns, Laser engineering of biomimetic surfaces, *Mater. Sci. Eng. R Rep.* 141 (2020) 100562.
- [11] X. Yuan, C. Yan, Y. Huang, Y. Tang, G. Chen, S. Zhang, High-performance bioinspired hierarchical microgroove wick for ceramic vapor chambers achieved by nanosecond pulsed lasers, *Langmuir* (2024).
- [12] G. Huang, J. Liao, C. Fan, S. Liu, W. Miao, Y. Zhang, S. Ta, G. Yang, C. Cui, Gradient-pattern micro-grooved wicks fabricated by the ultraviolet nanosecond laser method and their enhanced capillary performance, *Micromachines* 15 (1) (2024) 165.
- [13] G. Bamorovat Abadi, M. Bahrami, The effect of surface roughness on capillary rise in micro-grooves, *Sci. Rep.* 12 (1) (2022) 14867.
- [14] G. Jiang, Z. Tian, X. Luo, C. Chen, X. Hu, L. Wang, R. Peng, H. Zhang, M. Zhong, Ultrathin aluminum wick with dual-scale microgrooves for enhanced capillary performance, *Int. J. Heat Mass Tran.* 190 (2022) 122762.
- [15] L. Chen, Y. Xu, P. Bennett, J. Cheng, Q. Yang, D. Liu, Capillary performance of vertically grooved wicks on laser-processed aluminum surfaces with different wettability, *J. Phys. Appl. Phys.* 56 (42) (2023) 425501.
- [16] A. Samanta, W. Huang, H. Chaudhry, Q. Wang, S.K. Shaw, H. Ding, Design of chemical surface treatment for laser-textured metal alloys to achieve extreme wetting behavior, *ACS Appl. Mater. Interfaces* 12 (15) (2020) 18032–18045.
- [17] R. Fang, H. Zhang, J. Zheng, R. Li, X. Wang, C. Luo, S. Yang, S. Li, C. Li, Y. Chen, High-temperature silicon carbide material with wicking and evaporative cooling functionalities fabricated by femtosecond laser surface nano/microstructuring, *Ceram. Int.* 49 (12) (2023) 20138–20147.
- [18] R. Fang, X. Zhang, J. Zheng, Z. Pan, C. Yang, L. Deng, R. Li, C. Lai, W. Yan, V. S. Maisotsenko, Superwicking functionality of femtosecond laser textured aluminum at high temperatures, *Nanomaterials* 11 (11) (2021) 2964.
- [19] R. Fang, H. Zhu, Z. Li, X. Zhu, X. Zhang, Z. Huang, K. Li, W. Yan, Y. Huang, V. S. Maisotsenko, Temperature effect on capillary flow dynamics in 1D array of open nanotextured microchannels produced by femtosecond laser on silicon, *Nanomaterials* 10 (4) (2020) 796.
- [20] N.G. Tran, D.-M. Chun, Green manufacturing of extreme wettability contrast surfaces with superhydrophilic and superhydrophobic patterns on aluminum, *J. Mater. Process. Technol.* 297 (2021) 117245.
- [21] A. Samanta, W. Huang, A.S. Parveg, P. Kotak, R.C. Auyeung, N.A. Charipar, S. K. Shaw, A. Ratner, C. Lamuta, H. Ding, Enabling superhydrophobicity-guided superwicking in metal alloys via a nanosecond laser-based surface treatment method, *ACS Appl. Mater. Interfaces* 13 (34) (2021) 41209–41219.
- [22] J. Long, Y. Li, Z. Ouyang, M. Xi, J. Wu, J. Lin, X. Xie, A universal approach to recover the original superhydrophilicity of micro/nano-textured metal or metal oxide surfaces, *J. Colloid Interface Sci.* 628 (2022) 534–544.
- [23] J. Lee, Y. Suh, P.P. Dubey, M.T. Barako, Y. Won, Capillary wicking in hierarchically textured copper nanowire arrays, *ACS Appl. Mater. Interfaces* 11 (1) (2018) 1546–1554.
- [24] M. Stange, M.E. Dreyer, H.J. Rath, Capillary driven flow in circular cylindrical tubes, *Phys. Fluid.* 15 (9) (2003) 2587–2601.
- [25] R.K. Lade Jr., E.J. Hippchen, C.W. Macosko, L.F. Francis, Dynamics of capillary-driven flow in 3D printed open microchannels, *Langmuir* 33 (12) (2017) 2949–2964.
- [26] W.S. Yang, C.-J.C.J. Kim, Structured Surfaces with Engineered Wettability: Fundamentals, Industrial Applications, and Challenges for Commercialization, Springer, 2021.